

Time-Variant Radio Map Reconstruction with Optimized Distributed Sensors in Dynamic Spectrum Environments

Abstract—Radio environment maps (REMs) have been used to visualize the information of invisible electromagnetic spectrum. Although in the past there have been many research activities dealing with the reconstruction of static REMs, they did not consider the time variation of the dynamic spectrum operational environment. In this paper, we present a novel time-variant REM reconstruction methodology based on sparsely distributed sensors which jointly considers sensor layout optimization, propagation model improvement, and missing spectrum data recovery. To improve the sampling efficiency, the positions of sensors are first optimized based on a greedy-matching strategy and a gradient descend method. Then, by using the sampled spectrum data obtained from these sensors, the accuracy of commonly employed propagation models is improved and subsequently used to construct a channel dictionary for such time-varying environments. By exploring the heterogeneity of dynamic spectrum operational environments, an improved optimal reconstruction method is designed to recover the spectrum data using their spatial-temporal correlation. By considering a typical university campus environment as a case study, simulation and measurement data are obtained to reconstruct the time-variant REM. Through the simulation data, the reconstruction performance results are compared with those obtained from other state-of-the-art methods showing that the proposed methodology outperforms the others with respect to the sampling scheme and missing rate. Additionally, field measurement results have demonstrated that the proposed approach can effectively reconstruct time-variant REMs under dynamic scenarios.

Index Terms—Time-variant radio environment map, distributed sensor deployment, propagation model, REM reconstruction, compression sensing.

I. INTRODUCTION

A. Background and Previous Works

WITH the rapid increase in the massive use of electronic devices for various broadcasting, radar, and navigation system applications, the operation of wireless communication systems in complex electromagnetic environments has become increasingly perplex and challenging [1]–[3]. To deal with the scarcity of spectrum resources, the Federal Communications

Commission (FCC) has proposed the employment of cognitive radio (CR) technology as a possible solution [4]. Meanwhile, the Defense Advanced Research Projects Agency (DARPA) has introduced the radio environment map (REM), also known as the spectrum environment map (SEM), to provide a new and convenient way of displaying the availability of spectrum resources [5]. The REM can enable the visualization of important spectrum usage data information on geographical maps, such as spectrum usage in terms of time, frequency, received signal strength (RSS), and radio emitter position. Such visualization is very convenient and can be easily identify abnormal spectral activity, radio emitter localization, spectrum resource management, *etc.* [6]–[8]. A key challenge in the development of accurate REM is to recover the necessary data from the available sets of limited data obtained from undersampled geographical positions. For this reason, the reconstruction of accurate REMs under the constraint of limited sensors and sampling time has been recognized as one of its most challenging tasks [9], [10]. Meanwhile, as it will be elaborated in the next subsection, most of the existing methods have considered only the problem of static REM reconstruction without considering the actual time-variation of the operating dynamic spectrum environment.

In general terms, the research topic of REM reconstruction has been thoroughly investigated in the past, e.g., see [11]–[30], mainly using two kinds of approaches, namely data-driven and model-driven methods. The former relies on the correlation of spectrum data, while the latter utilizes the channel propagation model and the hidden information of RF emitters to reconstruct REMs.

For the data-driven methods, the spatial interpolation technique has been widely used to recovery missing data by directly mining the spatial correlation of sampled data [11], [12]. Two typical methods used in the past include inverse distance weighting (IDW) and the Kriging based approach [13], [14]. Further research efforts have dealt with multidimensional correlation of spectrum data, known as low rank characteristics, and have developed tensor/matrix completion techniques, e.g., see [15]–[18]. In particular, the concept of spectrum tensor to depict the multi-dimensional spectrum data was presented in [15] where a joint tensor completion scheme was developed. In [16], the authors proposed a framework to recover the spectrum occupancy matrix by minimizing the rank of sub-matrices. In [17], an approach to minimize the tensor rank and enforce the smoothness of spectrum map was introduced. The authors in [18] proposed a coupled tensor decomposition-based method for spectrum data completion.

Meanwhile, machine learning (ML) techniques have also

This work was supported in part by the National Natural Science Foundation of China under No. 62271250 and No. U23B2005, in part by Natural Science Foundation of Jiangsu Province under No. BK20211182, in part by the Key Technologies R&D Program of Jiangsu (Prospective and Key Technologies for Industry) under No. BE2022067, and BE2022067-3, BE2022067-1.

Qianhao Gao, Quiuming Zhu, Zhipeng Lin, Yi Zhao, Yang Huang, Jie Wang, and Qihui Wu are with The Key Laboratory of Dynamic Cognitive System of Electromagnetic Spectrum Space, College of Electronic and Information Engineering, Nanjing University of Aeronautics and Astronautics, 211106, Nanjing, China. (Email: qianhaogao, zhuqiuming, linlp, zhaoyi, yang.huang.ceie, bx2104906wangjie@nuaa.edu.cn, wuqihui2014@sina.com)

P. Takis Mathiopoulos is with the Department of Informatics and Telecommunications, National and Kapodistrian University of Athens, 15784 Athens, Greece. (Email: mathio@di.uoa.gr)

been recently adopted for the data-driven REM reconstruction, e.g., see [19]–[24]. These techniques typically treat the recovery of recast spectrum data as a learning-based optimization problem. For example, in [19] a solution was proposed by employing a network model which is trained with the available sampled data. Since the data structure of REMs resembled images, in [20] a propagation prediction model using convolutional neural networks (CNN) was introduced to recover the radio map. In another approach, the authors in [21] presented a low-complexity deep-learning based approach based on long-short term memory (LSTM) cells under urban and highway scenarios. The combination of deep learning with nonnegative matrix factorization methods to improve the reconstruction effectiveness was proposed in [22]. In addition, the authors in [23] introduced a power spectrum maps estimation method based on graph neural network (GNN) while the authors in [24] generated the radio map via a novel adversarial learning method.

On the other hand, for the model-driven methods the usual approach is to first estimate the information of radiation sources by the sampled data and then complete the missing data with the help of signal propagation models [25]. It is noted that compressed sensing (CS) has been also used in conjunction with model driven methods to recover the REM with sparse sampling data, e.g. see [26]–[30]. In particular, the authors in [26] proposed a CS-based wideband REM cartography to reduce the resource consumption. In [27], a CS-based multispectral cartography was proposed for spectrum sensing while in [28] the authors proposed a compressed REM mapping method based on the improved orthogonal matching pursuit (OMP) algorithm. In addition, the authors in [29], [30] proposed a sparse Bayesian learning based REM reconstruction algorithm to reduce the required spectrum data and achieve higher accuracy with low sampling rates.

It is underlined that the aforementioned works have mostly assumed that the spectrum environment is static with a few exceptions where it has been considered that it has quasi-static characteristics. For the most realistic case where the spectrum is time-variant only a few publications studying the reconstruction of REMs exist. In particular, the authors in [31] introduced a semi-supervised learning-based approach to construct time-variant REM by jointly considering the spatial and temporal trustworthiness. In [32], the authors adopted diffusion method together with a distance metric and introduced a correlation-based clustering to more accurately interpolate missing data. It is noted that these two methods can be viewed as an upgraded spatial interpolation approach. In [33], although the hidden spatial-temporal-spectral structures of the spectrum data have been exploited, the authors have modelled the time-variant REM as 3rd-order spectrum tensor without considering the statistics of the propagation model. The authors in [34] extracted the spatial propagation properties from the spatial-temporal spectrum data based on the proper orthogonal decomposition (POD) and proposed a greedy sampling locations optimization. Although this approach improves the REM reconstruction performance, it has serious disadvantages as it requires large amounts of prior data and does not consider the heterogeneity of space and time dimensions. In

another effort, the authors in [35] proposed an REM updating mechanism based on siamese neural networks (SNN) and the attention mechanism, which nevertheless requires massive data to train the network model. Finally, [36] has presented an effort to combine the optical flow vectors field with the radiation sources movement vectors, and used the channel model driven extrapolation method to predict the REMs. However, this approach ignored the spatial characteristics of REM data and required some prior data.

Based upon the previous discussion, and to the best of our knowledge, we can conclude that there has been no paper published in the open technical literature which addresses in a systematic manner the challenging problem of optimizing the performance of time-variant REM.

B. Contributions

Motivated by the previous observations, in this paper we propose a novel time-variant REM reconstruction methodology based on CS concepts, which holistically considers the optimization of sensor layout, the impact of channel propagation models, and the inherent spatial-temporal heterogeneity of spectrum data. Within this framework, the main novel contributions of this paper can be summarized as follows.

- 1) A greedy-matching based sensor layout optimization algorithm is developed. The sensing matrix is first obtained by a gradient descent method, and then the sensor position is iteratively determined and optimized by an upgraded greedy matching algorithm. The proposed model-driven method has very high sampling efficiency and low reconstruction error.

- 2) An environment-dependent propagation model dictionary is developed to improve the reconstruction accuracy. By using the sampled data to iteratively optimize the close-in (CI) model and/or other well-known channel models like the Hata and ITU models, the proposed approach considers various environmental factors including the effects of buildings, vegetation, and signal shadowing. Such information combined with the estimated information of sparse radio frequency (RF) emitters, naturally leads to the accurate recovery of missing data in the spatial zone which will improve the overall reconstruction performance.

- 3) By considering the heterogeneity of spectrum data in dynamic operational environments, a novel data recovery method based upon a spatial-temporal joint semi-variogram is proposed to depict the inherent data correlation. The proposed method overcomes the restrictive condition of homo-distribution of spatial-temporal data required by traditional methods and exhibits excellent spectrum data recovery performance.

The rest of this paper is organized as follows. After this introduction, Section II presents the system model and by using CS formulates the problem of REM reconstruction. In Section III, the details of the proposed time-variant reconstruction methodology are presented. Section IV presents performance evaluation results by simulations and field measurement data. The conclusions of the paper can be found in Section V.

II. SYSTEM MODEL AND PROBLEM DEFINITION

In this section, first the overall system and time-variant REM models is presented. Then, appropriate mathematical

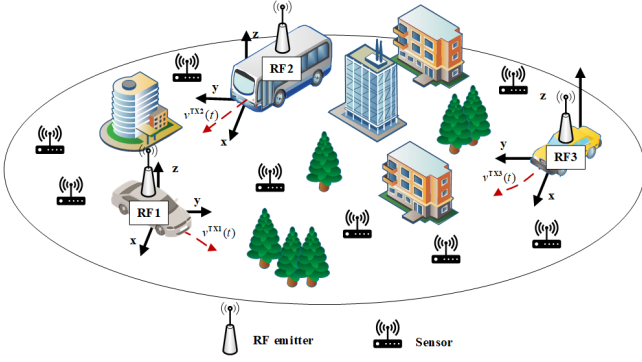


Fig. 1: The considered system model and its time-variant REM operation in a dynamic spectrum environment.

formulations related with the CS problem are introduced, which would be used to recover the REM with sparse sampling data.

A. System and Time-variant REM Models

Fig. 1 illustrates the dynamic spectrum environment in which the considered REM is assumed to operate. It consists of several mobile RF emitters and some sensors, which are sparsely distributed in the coverage area as well as various obstacles, such as buildings and trees. The REM which will be studied is a received signal strength (RSS) map, which is also referred to as “spectrum map”.

By displaying typical measured data, Fig. 2 illustrates the three operational steps of the proposed time-variant REM reconstruction process, namely the “Sampling Position”, “Sampled Data” and “Reconstructed REM”. In the “sampling position” part, the region of interest (ROI), shown with squares, is first discretized into a set of small grids. Then, in the “sampled data” part, distributed sensors are arranged in the center of the sensor layout scheme to obtain the RSS value of the entire grid. In the “reconstructed REM” part, the RSS values of the unsampled grid are estimated or recovered to reconstruct the REM.

For this system model, it is assumed that the available RF emitters are mobile, and due to the fading phenomenon, the time-variant REM can be described within a time period as a 3rd-order tensor $\mathcal{X} \in \mathbb{R}^{N_x \times N_y \times N_t}$. As also shown in Fig. 2, N_x and N_y represent the maximum number of grid index along the x-y axis respectively, and N_t indicates the one along the time index. The element of grid (n_x, n_y) at the n_t^{th} timeslot can be denoted as $x(n_x, n_y, n_t)$. Note that \mathcal{X} can also be viewed as a sequence of 2D slice, which represents the space REM for each timeslot as $\mathcal{X} = [\mathbf{X}_1, \mathbf{X}_2, \dots, \mathbf{X}_{N_t}]$.

The sampling positions at the n_t^{th} timeslot can be mathematically expressed by the following matrix

$$C_{n_t}(n_x, n_y) = \begin{cases} 1, & \text{if a sensor is at grid } (n_x, n_y), \\ 0, & \text{otherwise.} \end{cases} \quad (1)$$

Furthermore, the time-variant sampling positions can be expressed by a tensor, $\mathcal{C} = [\mathbf{C}_1, \mathbf{C}_2, \dots, \mathbf{C}_{N_t}]$, whereas the raw spectrum data collected from these positions can be obtained as

$$\tilde{\mathcal{X}} = \mathcal{X} \otimes \mathcal{C}, \quad (2)$$

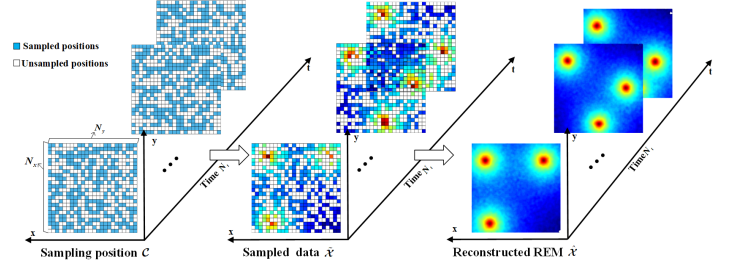


Fig. 2: A typical illustration of the time-variant REM reconstruction process based upon measured data.

where \otimes represents the matrix Hadamard product.

The main challenge in REM reconstruction is to recover the REM tensor $\hat{\mathcal{X}}$, based on the sampled raw data $\tilde{\mathcal{X}}$. This can be accomplished through the minimization of the difference between $\hat{\mathcal{X}}$ and \mathcal{X} as

$$\begin{aligned} \min & \|\hat{\mathcal{X}} - \mathcal{X}\|_F \\ &= \|(\hat{\mathbf{X}}_1 - \mathbf{X}_1); (\hat{\mathbf{X}}_2 - \mathbf{X}_2); \dots; (\hat{\mathbf{X}}_{N_t} - \mathbf{X}_{N_t})\|_F, \\ \text{s.t. } & \hat{\mathcal{X}} \otimes \mathcal{C} = \tilde{\mathcal{X}}, \end{aligned} \quad (3)$$

where $\|\cdot\|_F$ denotes the Frobenius norm, which calculates the square root of the sum of the absolute square of tensor's elements.

B. Compressed Sensing based REM Data Recovery

As the RF emitters shown in Fig. 2 are assumed to be sparsely distributed in the ROI, CS can achieve high reconstruction performance by exploiting sparsity. Therefore, the reconstruction of the n_t^{th} REM, i.e., the spectrum matrix \mathbf{X}_{n_t} , can be formulated as a CS problem which will be solved next in order to recover the values of all $N_{xy} = N_x \times N_y$ grids at the n_t^{th} timeslot.

Let us first consider a sparse signal vector $\omega_{n_t} = [\omega_{n_t,1}, \omega_{n_t,2}, \dots, \omega_{n_t,n_{xy}}, \dots, \omega_{n_t,N_{xy}}]$ where

$$\omega_{n_t,n_{xy}} = \begin{cases} P_{n_t,n_{xy}}^t, & \text{if an emitter is at grid } n_{xy}, \\ 0, & \text{else,} \end{cases} \quad (4)$$

with $P_{n_t,n_{xy}}^t$ being the transmitting power of the RF emitter at grid n_{xy} at time n_t . Clearly, if there exist K RF emitters, ω_{n_t} is a K -sparse signal vector. The RSS $P_{n_t,n'_{xy},k}^r$ from the k^{th} RF emitter to the sensor at grid n'_{xy} can be expressed as

$$P_{n_t,n'_{xy},k}^r = \varphi_{n'_{xy},k} P_{n_t,k}^t, \quad (5)$$

where $\varphi_{n'_{xy},k}$ is the propagation gain from the k^{th} emitter to the n'_{xy} grid, and $P_{n_t,k}^t$ denotes its transmitting power. Since the RSS measured by each sensor may include the receiving power of several RF transmitters, the total RSS at grid n'_{xy} can be obtained as

$$x_{n'_{xy},n_t} = \sum_{k=1}^K P_{n_t,n'_{xy},k}^r + \varepsilon, \quad (6)$$

where ε is the measurement noise.

Equivalently, this can be written as

$$\mathbf{x}_{n_t} = \varphi \cdot \omega_{n_t} + \varepsilon, \quad (7)$$

where $\mathbf{x}_{n_t} \in \mathbb{R}^{N_{xy} \times 1}$ is obtained by vectorizing the spectrum matrix $\mathbf{X}_{n_t} \in \mathbb{R}^{N_x \times N_y}$, $\boldsymbol{\omega}_{n_t} \in \mathbb{R}^{N_{xy} \times 1}$ is the sparse signal and $\boldsymbol{\varphi} \in \mathbb{R}^{N_{xy} \times N_{xy}}$ is the channel propagation dictionary which is defined as the propagation channel characteristic between the grids. For instant, the element $\varphi_{n'_{xy}, n_{xy}}$ in the n'_{xy} th row and the n_{xy} th column can be expressed as

$$\varphi_{n'_{xy}, n_{xy}} = 10 \log_{10} \frac{(4\pi d_{n'_{xy}, n_{xy}})^2}{G_{n'_{xy}} G_{n_{xy}} \lambda^2} + 10 \xi \log_{10}(d_{n'_{xy}, n_{xy}}) + \chi_{\sigma}^{\text{CI}}, \quad (8)$$

where λ is the propagation signal wavelength, $G_{n_{xy}}$ and $G_{n'_{xy}}$ are the antenna gains of the emitter at grid n_{xy} and the sensor at grid n'_{xy} , respectively, $d_{n'_{xy}, n_{xy}} = \|\mathbf{L}'_{xy} - \mathbf{L}_{xy}\|_2$ is the distance between the grid n_{xy} and the grid n'_{xy} , ξ is path loss exponent, and $\chi_{\sigma}^{\text{CI}}$ is a zero-mean Gaussian random variable with a standard deviation σ . It is noted that previously published papers, e.g., [26], have used simplified channel models which do not consider various scattering phenomena, such as reflection and diffraction. Thus, it is necessary to enhance such propagation dictionaries to capture propagation features in the spectrum environment so that the REM reconstruction performance can be improved.

For this purpose, it is necessary to use a vectorized sampled spectrum data set. At the time n_t , the measurement matrix, which identifies the position of the sensors, can be expressed as

$$\boldsymbol{\psi}_{n_t} = \boldsymbol{\Sigma} \otimes [\mathbf{E}_{n_t}, \mathbf{E}_{n_t}, \dots, \mathbf{E}_{n_t}]^T, \quad (9)$$

where $\boldsymbol{\Sigma}$ is an $N_{xy} \times N_{xy}$ identity matrix. Each row of $\boldsymbol{\psi}_{n_t}$ has an element of 1 denoting the sampled position in the ROI and \mathbf{E}_{n_t} can be expressed as

$$\mathbf{E}_{n_t} = \begin{bmatrix} [1, 0, 0, \dots, 0] \cdot \mathbf{C}_{n_t} & [0, 1, 0, \dots, 0] \cdot \mathbf{C}_{n_t} & \dots \\ [0, 0, 0, \dots, 1] \cdot \mathbf{C}_{n_t} & & \end{bmatrix}^T. \quad (10)$$

Finally, the vectorized sampled spectrum data at time n_t can be obtained as

$$\tilde{\mathbf{x}}_{n_t} = \boldsymbol{\psi}_{n_t} \boldsymbol{\varphi} \boldsymbol{\omega}_{n_t} + \boldsymbol{\varepsilon}. \quad (11)$$

III. REM RECONSTRUCTION METHODOLOGY

This section presents the details of the proposed methodology for obtaining the new time-variant REM reconstruction scheme. After discussing the operational details of the system model, a greedy-matching based sensor layout optimization algorithm which enhances the efficiency of spectrum data acquisition is introduced. By considering the effects of buildings, shadowing, and antenna pattern [37] on the received signal power, the propagation channel and sampled data are combined to obtain a realistic propagation model for the intra-slice recovery. For the inter-slice recovery, a spatial-temporal semi-variance function is introduced to more accurately model the spectrum data correlation of different time instants in dynamic scenarios.

A. An Overview of Proposed REM Reconstruction Methodology

Fig. 3 illustrates the block diagram of the proposed REM reconstruction methodology which consists of three main modules: i) The sensor layout optimization (SLO); ii) The

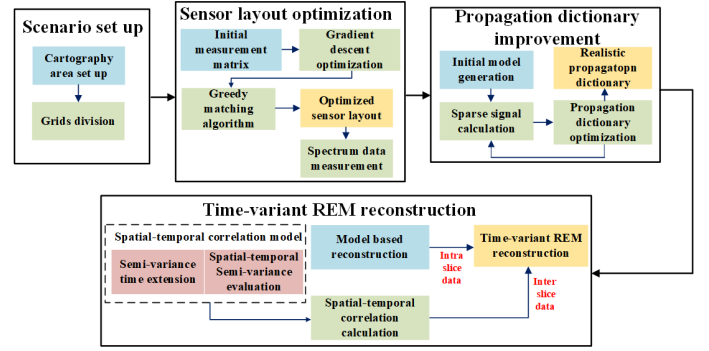


Fig. 3: The detailed block diagram of the proposed time-variant REM reconstruction methodology.

propagation dictionary improvement (PDI); and iii) The time-variant REM reconstruction (TVR). Firstly, the gradient descent method and the upgraded greedy matching algorithm are jointly used to optimize the sensor position (measurement matrix) to obtain a better spatial distribution. Secondly, based on the previously described CS approach, the sparse signal is recovered by the sampled data, which are then being used to correct and update initial propagation model dictionary. Through continuous iterations, the propagation dictionary can be made more suitable for the under consideration environment. Finally, by considering the heterogeneity of spectrum data, we extend the semi-variance function to the time domain and evaluate the spatial-temporal semi-variance to obtain spatial-temporal correlation. Combining the optimized dictionary used for intra-slice recovery with spatial-temporal correlation used for inter-slice recovery, the time-variant REM is reconstructed.

B. Distributed Sensor Layout Optimization

It has been shown that by reducing the correlation between the propagation dictionary and the sensor position (or measurement matrix), improved reconstruction performance can be obtained [27]. Thus, by reducing this correlation the measurement matrix will be optimized. This, in turn, will make the compressed sensing process more consistent with the restricted isometry property (RIP), thereby improving the accuracy of reconstruction [28]. Let define the correlation coefficient $\rho(\mathbf{S})$ as

$$\rho(\mathbf{S}) = \max_{i \neq j} \left\{ \frac{|s_i^T s_j|}{\|s_i\| \|s_j\|} \right\}, \quad (12)$$

where $\mathbf{S} = \boldsymbol{\psi} \boldsymbol{\varphi}$ is the sensing matrix, $\boldsymbol{\psi}$ denotes the position of sensors, $\boldsymbol{\varphi}$ is the channel dictionary matrix, and s_i^{th} is the i^{th} column of \mathbf{S} .

Clearly, since Eq. (12) is the worst-case bound which is difficult to solve, it's convenient to be transformed into a more trackable optimization model [4]. In particular, letting $\mathbf{G} = \mathbf{S}^T \mathbf{S}$, the correlation coefficient can also be viewed as the maximum absolute value of non-diagonal elements in \mathbf{G} which makes it an approximate identity matrix

$$\mathbf{G} = \mathbf{S}^T \mathbf{S} = \boldsymbol{\varphi}^T \boldsymbol{\psi}^T \boldsymbol{\psi} \boldsymbol{\varphi} \approx \mathbf{I}, \quad (13)$$

where \mathbf{I} is an identity matrix.

Thus, the problem of sensor position optimization is now transformed into an unconstraint optimization problem which can be conveniently expressed as

$$\hat{\psi} = \arg \min_{\psi} \|\varphi^T \psi^T \psi \varphi - \mathbf{I}\|_F^2, \quad (14)$$

Its optimal solution can be conveniently obtained using the gradient descent method. For this, let us first define the error function as $J(\psi) = \|\varphi^T \psi^T \psi \varphi - \mathbf{I}\|_F^2$ and take the derivative of measurement matrix as

$$\begin{aligned} \frac{\partial J(\psi)}{\partial \psi} &= \frac{\partial}{\partial \psi} \left\{ \text{tr}[(\varphi^T \psi^T \psi \varphi - \mathbf{I})^T (\varphi^T \psi^T \psi \varphi - \mathbf{I})] \right\} \\ &= 4\psi \varphi (\varphi^T \psi^T \psi \varphi - \mathbf{I}) \varphi^T, \end{aligned} \quad (15)$$

where $\text{tr}(\cdot)$ is the trace of the matrix.

Then, a gradient descent approach can be used to optimize the measurement matrix as

$$\begin{aligned} \psi_{iter+1} &= \psi_{iter} - \beta \frac{\partial J(\psi)}{\partial \psi} \\ &= \psi_{iter} - \eta \psi_{iter} \varphi (\varphi^T \psi^T \psi \varphi - \mathbf{I}) \varphi^T, \end{aligned} \quad (16)$$

where the iteration step is set as $\eta = 4\beta$ ($\beta > 0$) and $iter$ is the iteration index.

Note that through the optimized measurement matrix alone the sensor positions cannot be directly obtained. Thus, next we propose a novel greedy matching based algorithm to select proper positions. It is first noted that the layout process of sensor is essentially a binary selection procedure, and by placing a new sensor, a column is selected from the channel dictionary matrix. In the proposed algorithm the position that is closest to the optimized sensing matrix is selected as the new sensor position. Furthermore, by imposing a distance constraint to avoid the selection of adjacent positions, the optimization objective for the i^{th} sensor can be mathematically expressed as

$$\begin{aligned} \min_{\psi} & \|\psi(l, :) \varphi - \hat{S}(l, :)\|_F^2, \\ \text{s.t. } & \psi_{lj} \in \{0, 1\}, j = 1, 2, \dots, n, \hat{\mathbf{S}} = \hat{\psi} \varphi, \end{aligned} \quad (17)$$

where $\hat{\psi}$ is the final measurement matrix. The algorithmic implementation of the proposed algorithm is shown in Algorithm 1. Finally, the optimized positions of distributed sensors can be obtained from the measurement matrix.

C. Propagation Dictionary and Sparse RF emitters Estimation

The propagation models commonly adopted for REM reconstruction are the free-space propagation model and/or other well-known channel models such as the Hata and ITU models. Unfortunately, these models are not capable of accurately considering specific characteristics of practical propagation environments, and unavoidably their use will lead to inaccurate REM reconstruction. To deal with this problem, in our paper we improve the propagation modelling procedure by employing measured sparse data, which clearly are more accurate as they include the characteristics of ROI.

The initial propagation dictionary is built based on the CI channel model and Eq. (8). The sparse signal ω_{n_t} can be first

Algorithm 1 Greedy-matching based sensor position selection algorithm

Input: Channel dictionary φ , Optimized sensing matrix $\hat{\mathbf{S}}$, number of sensors m .

Output: Sensor set Ω , Measurement matrix ψ .

```

1: for  $i \in [1, m]$  do
2:   Initialize temporary variable  $\mathbf{T} = \emptyset$ ,  $idx = 0$ .
3:   for  $j \in [1, n]$  do
4:      $\mathbf{T} = \mathbf{T} \cup \|\varphi(j, :) - \hat{\mathbf{S}}(i, :)\|_F^2$ 
5:   end for
6:    $idx =$  The index of the minimum in temporary variable  $\mathbf{T}$ .
7:    $\Omega = \Omega \cup idx$ .
8:   Initialize Adjacency set  $\mathbf{A} = \emptyset$ , obtain the index of adjacent positions with  $idx$ .
9:   for  $k \in [1, n]$  do
10:    if Distance( $k, idx$ )  $< 2$  then
11:       $A = A \cup k$ , append  $k$  into adjacency set.
12:    end if
13:  end for
14:   $\varphi(A, :) = +\infty$ 
15: end for
16: Map the sensor set to measurement matrix  $\Omega \rightarrow \psi$ .
17: return Sensor set  $\Omega$ , measurement matrix  $\psi$ .
```

estimated by the spectrum data sampled by the sensors. Then, both the sparse signal ω_{n_t} and the propagation dictionary φ are iteratively improved by a matrix decomposition technique.

The sparse signal recovery can be equivalent to an l_1 minimization problem as

$$\begin{aligned} \hat{\omega}_{n_t} &= \arg \min_{\omega_{n_t}} \|\omega_{n_t}\|_1, \\ \text{s.t. } & \|\tilde{\mathbf{x}}_{n_t} - \psi_{n_t} \varphi \omega_{n_t}\| \leq \varepsilon, \end{aligned} \quad (18)$$

where $\tilde{\mathbf{x}}_{n_t}$ is the sampled spectrum data vector and ε is the measurement error. Since Eq. (18) can be considered as an l_1 regularized linear regression problem, the objective of optimization can be rewritten as

$$\hat{\omega}_{n_t} = \arg \min_{\omega_{n_t}} \frac{1}{2} \|\tilde{\mathbf{x}}_{n_t} - \psi_{n_t} \varphi \omega_{n_t}\|^2 + \eta \|\omega_{n_t}\|_1, \quad (19)$$

where η is a scalar regularization parameter.

The alternating direction method of multipliers (ADMM) is used to transform the objective function into two separable variables. This simplifies the l_1 minimization problem which can be rewritten as

$$\begin{aligned} \min & f(\omega_{n_t}) + g(\mu), \\ \text{s.t. } & \omega_{n_t} - \mu = 0, \end{aligned} \quad (20)$$

where $f(\omega_{n_t}) = \frac{1}{2} \|\tilde{\mathbf{x}}_{n_t} - \psi_{n_t} \varphi \omega_{n_t}\|^2$ and $g(\mu) = \eta \|\mu\|_1$. Thus, the variables can be updated as

$$\begin{aligned} \omega_{n_t}^{l+1} &= (\varphi^T \psi_{n_t}^T \psi_{n_t} \varphi + \rho \Sigma)^{-1} \\ & \quad (\varphi^T \psi_{n_t}^T \tilde{\mathbf{x}}_{n_t} + \rho(\mu^l - \mathbf{u}^l)), \\ \mu^{l+1} &= S_{\eta/\rho}(\omega_{n_t}^{l+1} + \mathbf{u}^l), \\ \mathbf{u}^{l+1} &= \mathbf{u}^l + \omega_{n_t}^{l+1} - \mu^{l+1}, \end{aligned} \quad (21)$$

where $\rho > 0$ and $S_{\eta/\rho}(\cdot)$ is the soft thresholding function.

Furthermore, instead of only considering the sparse solution ω_{n_t} , we jointly optimize φ and ω_{n_t} in order to improve the accuracy, which can be expressed as

$$\begin{aligned} & \|\mathbf{x}_{n_t} - \tilde{\psi}_{n_t} \varphi \omega_{n_t}\| \\ &= \|\mathbf{x}_{n_t} - \sum_{j=1}^{N_{xy}} \varphi(\cdot, j) \omega_{n_t}(j)\| \\ &= \|(\mathbf{x}_{n_t} - \sum_{j \neq i} \varphi(\cdot, j) \omega_{n_t}(j)) - \varphi(\cdot, i) \omega_{n_t}(i)\|, \end{aligned} \quad (22)$$

where $\mathbf{x}_{n_t} = \varphi \omega_{n_t}$ and $\tilde{\psi}_{n_t}$ is degenerated to the identity matrix.

The optimization problem can then be conveniently expressed as

$$\begin{aligned} \hat{\varphi}, \hat{\omega}_{n_t} &= \arg \min_{\varphi, \omega_{n_t}} \|(\mathbf{H}_i - \varphi(\cdot, k) \omega_{n_t}(k))\|, \\ \text{s.t. } \mathbf{H}_i &= \mathbf{x}_{n_t} - \sum_{j \neq i} \varphi(\cdot, j) \omega_{n_t}(j). \end{aligned} \quad (23)$$

Finally, we can use singular value decomposition (SVD) to solve the Eq. (23), which can be iterated as

$$\begin{aligned} \mathbf{H}_i &= \mathbf{U} \mathbf{\Omega} \mathbf{V}^T, \\ \varphi(\cdot, k) &= \mathbf{U}(\cdot, 1), \\ \omega_{n_t}(k) &= \mathbf{\Omega}(1, 1) \mathbf{V}^T(1, \cdot), \end{aligned} \quad (24)$$

where $\mathbf{\Omega}$ is singular value diagonal matrix, and \mathbf{U} and \mathbf{V} are unitary matrices.

D. Time-variant REM Reconstruction

Let us denote the sampled data as $\tilde{x}_i, i = 1, 2, M$ and $M = \|\tilde{\mathcal{X}}\|_0$ as the total number of the data. By representing each element of spectrum tensor $\hat{\mathcal{X}}$ as \hat{x} , they can be obtained as

$$\hat{x} = \sum_{i=1}^M w_i \tilde{x}_i, \quad (25)$$

where w_i denotes the contribution of i th observed data. For the special case of recovering a unsampled position, the optimization objective of Eq. (3) can be rewritten as

$$\begin{aligned} & \min_{w_i} [\mathbb{E}(\hat{x} - x)]^2, \\ & \text{s.t. } \mathbb{E}(\hat{x} - x) = 0. \end{aligned} \quad (26)$$

To solve this unbiased estimation problem, the total space is assumed to be homogeneous, and that each sensor position has a different distance from RF emitters and thus is affected by different propagation channels. Therefore, the statistical expectation of each position varies as it gets influenced by the different propagation path losses and spatial spectrum distributions. This heterogeneity can be mathematically expressed as

$$b_i \mathbb{E}(x) = \mathbb{E}(\tilde{x}_i), \quad (27)$$

where b_i is the ratio between the sampled spectrum data and recovered one. The expectation of the unknown spectrum data can be obtained using Eq. (7) as

$$b_i(x) = \frac{\tilde{x}_i}{\varphi(x) \cdot \omega_{n_t}^T}, \quad (28)$$

where $\varphi(x)$ is the propagation dictionary row for the current x , and ω_{n_t} is the estimated vector of the RF emitters.

It is underlined that, as compared to the static case, this spatial-temporal heterogeneity makes the time-variant REM reconstruction a much more challenging problem to solve. Therefore, to recover the missing data, a spatial-temporal joint semi-variogram will be introduced next to depict the inherent correlation of spectrum data at different positions and time instants. Noting that, since the covariance of two positions relates to both distance and time domains, the time interval Δh_t and space interval Δh_s should be considered separately. Thus, we use the following spatial-temporal covariance

$$\begin{aligned} & R_{st}(\Delta h_s, \Delta h_t) \\ &= \text{Cov} \{ [x(\mathbf{L}_{xy} + \Delta h_s, n_t + \Delta h_t), x(\mathbf{L}_{xy}, n_t)] \} \\ &= \mathbb{E} \{ [x(\mathbf{L}_{xy} + \Delta h_s, n_t + \Delta h_t) - \mathbb{E}[x(\mathbf{L}_{xy} + \Delta h_s, n_t + \Delta h_t)] \\ & \quad [x(\mathbf{L}_{xy}, n_t) - \mathbb{E}[x(\mathbf{L}_{xy}, n_t)]] \}, \end{aligned} \quad (29)$$

where $\mathbf{L}_{xy} = (n_x, n_y)$ represents the spatial position with respect to of the time index n_t , Δh_s and Δh_t represent the space and time intervals, respectively, and $\text{Cov}[\cdot]$ is the correlation function.

Furthermore, as shown in Appendix A, the spatial-temporal semi-variance function can be expressed as

$$\begin{aligned} & \gamma_{st}(\Delta h_s, \Delta h_t) \\ &= \frac{1}{2} \mathbb{E} [x(\mathbf{L}_{xy} + \Delta h_s, n_t + \Delta h_t) - x(\mathbf{L}_{xy}, n_t)]^2 \\ &= \sigma_{st}^2 - R_{st}(\Delta h_s, \Delta h_t), \end{aligned} \quad (30)$$

where σ_{st}^2 is the variance of spatial-temporal spectrum data.

To obtain the optimal weights, the following optimization problem can be solved (see Appendix B for the derivation details)

$$\begin{aligned} \min \mathcal{L} &= - \sum_{i=1}^M \sum_{j=1}^M w_i w_j \gamma_{st}(\Delta h_{sij}, \Delta h_{tij}) \\ &+ 2 \sum_{i=1}^M w_i \gamma(\Delta h_{si0}, \Delta h_{ti0}), \\ \text{s.t. } &\sum_{i=1}^M w_i b_i = 1. \end{aligned} \quad (31)$$

Based on the Lagrangian, the constrained optimization problem can be rewritten as

$$\begin{aligned} \mathcal{L} &= - \sum_{i=1}^M \sum_{j=1}^M w_i w_j \gamma_{st}(\Delta h_{sij}, \Delta h_{tij}) \\ &+ 2 \sum_{i=1}^M w_i \gamma(\Delta h_{si0}, \Delta h_{ti0}) - 2\zeta (\sum_{i=1}^M w_i b_i - 1), \end{aligned} \quad (32)$$

where ζ is the Lagrange multiplier. By taking the partial derivatives of \mathcal{L} , the weights can be obtained by Eq. (33)

IV. PERFORMANCE EVALUATION RESULTS AND DISCUSSION

The section evaluates the performance of the proposed REM reconstruction methodology by means of computer simulations

$$\begin{bmatrix} w_1 \\ w_2 \\ \vdots \\ w_M \\ \zeta \end{bmatrix} = \begin{bmatrix} \gamma_{st}(\Delta h_{s11}, \Delta h_{t11}) & \cdots & \gamma_{st}(\Delta h_{s1M}, \Delta h_{t1M}) & b_1 \\ \vdots & \ddots & \vdots & \vdots \\ \gamma_{st}(\Delta h_{sM1}, \Delta h_{tM1}) & \cdots & \gamma_{st}(\Delta h_{sMM}, \Delta h_{tMM}) & b_M \\ b_1 & \cdots & b_M & 0 \end{bmatrix}^{-1} \begin{bmatrix} \gamma_{st}(\Delta h_{s10}, \Delta h_{t10}) \\ \gamma_{st}(\Delta h_{s20}, \Delta h_{t20}) \\ \vdots \\ \gamma_{st}(\Delta h_{sM0}, \Delta h_{tM0}) \\ 1 \end{bmatrix} \quad (33)$$

TABLE I: SIMULATION PARAMETERS.

Parameter	Value						
	Type	Number	Height (m)	Power (dBm)	Speed (m/s)	Antenna type	Antenna max gain (dBi)
RF emitter setting	Pedestrian	3	1.5	20	1	Isotropic	0
			1.5	20	1	Isotropic	0
			1.5	20	1	Isotropic	0
	Vehicle	2	1	20	5	Isotropic	0
			1	20	5	Isotropic	0
	Micro base station	2	20	20	0	Isotropic	0
			30	20	0	Directional	0
	Mobile radio	1	2	20	3	Isotropic	0
Center frequency	2.45 GHz						
Bandwidth	10 MHz						
Cartography area	1 km x 1 km						
Grid resolution	20 m x 20 m						
Update time interval	1 s						

and field measurement experiments. These have been carried out in a certain part of the Nanjing University of Aeronautics and Astronautics (NUAA) campus (see Fig. 4), which has been selected since it include various propagation environments as well as different types of buildings, roads, and unobstructed areas. For the former, we adopt the ray tracing (RT) technology to obtain computer simulated data. These data have been used to compare the reconstruction performance of the proposed scheme with that of other state-of-the-art schemes, so that its superiority of proposed methodology can be demonstrated. For the latter, we use the field measurement data to reconstruct the time-variant REM, which proves the effectiveness of proposed scheme for the spectrum cartography under dynamic scenarios.

A. RT-based simulation and comparison

In this section, the performance of proposed REM reconstruction methodology is verified by extensive computer-based simulations in the area of NUAA campus illustrated in Fig. 4. The covered area is about 1 km x 1 km wide and as it can be seen from the figure it includes different types of buildings, with heights from 19-55 m (average height is about 30 m) various trees, roads and empty spaces. The operation of the mobile RF emitters is implemented by mobile radios carried out by pedestrians and vehicles at different speeds following different routes as these are also indicated in Fig. 4. On the other hand, the operation of the fixed position RF emitters is implemented by base stations (including directional and isotropic radiation antennas). It is assumed that their transmitted power is 20 dBm (at 2450 MHz), and they are placed at different heights above the ground. The half-power beamwidth of the E and H planes of the employed directional antenna is 15 degrees, whereas

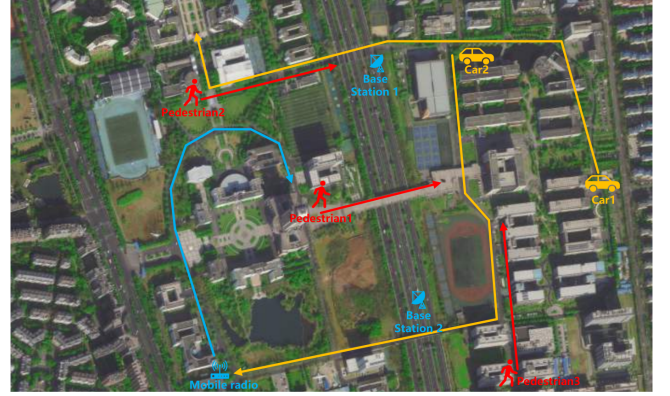


Fig. 4: A satellite picture view of the NUAA campus area where the experiments took place.

the first null beamwidth of the E and H planes is 60 degrees. Table I summarizes all the important simulation parameters used to obtain the computer simulated performance evaluation results. RT technology is used to estimate the ideal RSS values in each grid under this dynamic scenario and the simulated data tensor is 50 x 50 x 5.

The performance of the newly proposed REM methodology was compared with that of three baseline schemes, namely IDW [13], HaLRTC (high accuracy low rank tensor completion) [18], and Kriging [14], all of which have been extensively used for REM reconstruction. In addition, to further expand this comparison, we have used three data collection schemes, namely regularly distributed, random distributed, and vehicle mounted sensors.

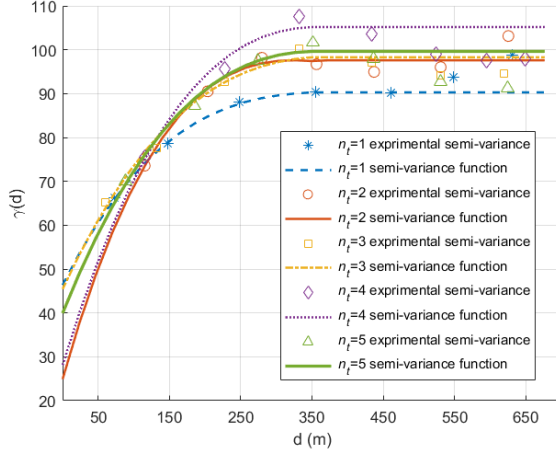


Fig. 5: Experimental spatial semi-variance values and fitted semi-variance function at five different time instants.

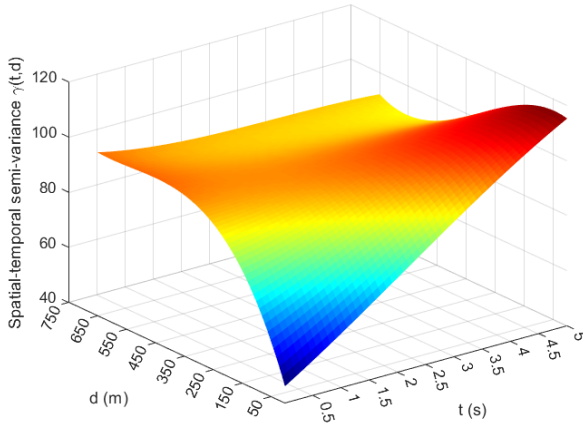


Fig. 6: Spatial-temporal semi-variance with different spatial distance and time intervals for time-variant REM.

Fig. 5 presents the experimental spatial semi-variance values and the fitted semi-variance function obtained by using Eq. (30) without considering the time domain at different time instant. It is clear from these results that the semi-variance function is slightly different at various time instant under the dynamic environment. Moreover, if the space interval is relatively small, i.e., $d < 250$ m, $\gamma(d)$ increases with increasing d . However, when the interval reaches the correlation distance, which is about 250-300 m for our simulation scenario, the semi-variance remains constant. This means that the spatial correlation of spectrum data become irrelevant when $d > 300$ m. Fig. 6 shows the spatial-temporal semi-variance $\gamma(t, d)$ as a function of the distance d and time intervals t for the time-variant REM by using Eq. (30). As it can be seen, when the values of d and t increase, the spatial-temporal semi-variance $\gamma(t, d)$ also increases, which indicates that the correlation between the spectrum data weakens with the increase of distance and time. For the spatial dimension, $\gamma(t, d)$ increases until d reaches 400 m and then it remain constant. While it exhibits a nearly linear

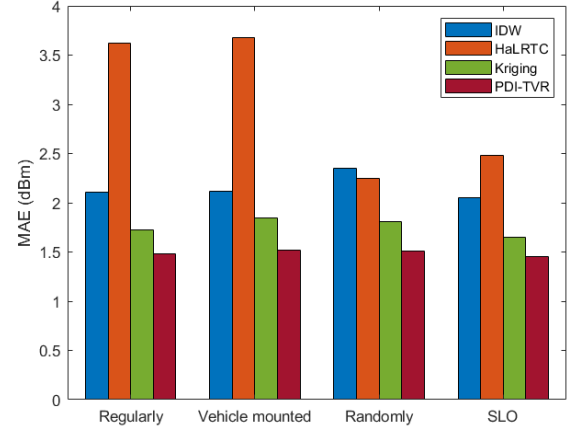


Fig. 7: Reconstruction performance comparisons of different methods with different sampling schemes.

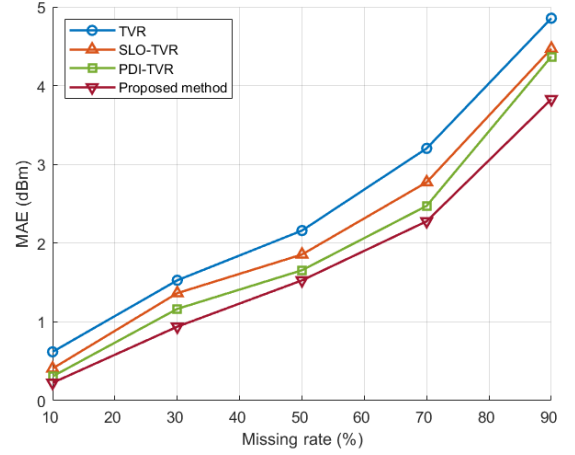


Fig. 8: Reconstruction performance about ablation study with different missing rates.

progression for the temporal dimension.

To further evaluate the REM reconstruction performance, the mean absolute error (MAE) [in dBm] criterion is adopted to estimate the reconstruction error, i.e.

$$\begin{aligned} \text{MAE(dBm)} &= \frac{\|\hat{\mathcal{X}} - \mathcal{X}\|_1}{N} \\ &= \frac{\|(\hat{\mathbf{X}}_1 - \mathbf{X}_1); (\hat{\mathbf{X}}_2 - \mathbf{X}_2); \dots; (\hat{\mathbf{X}}_T - \mathbf{X}_T)\|_1}{N}, \end{aligned} \quad (34)$$

where \mathcal{X} is the simulated (also considered as ideal) REM, $\hat{\mathcal{X}}$ is the constructed REM, and N is the grid number.

In Fig. 7, the MAE performance of the four sampling schemes under consideration with 50% (1250 sensors) missing data rate is compared. These results have shown that the MAE trends of different schemes are very similar for the different reconstruction methods. However, the proposed sensor layout optimization (SLO) scheme outperforms the other three schemes for most reconstruction methods, followed by the regularly layout scheme. Different from the other three

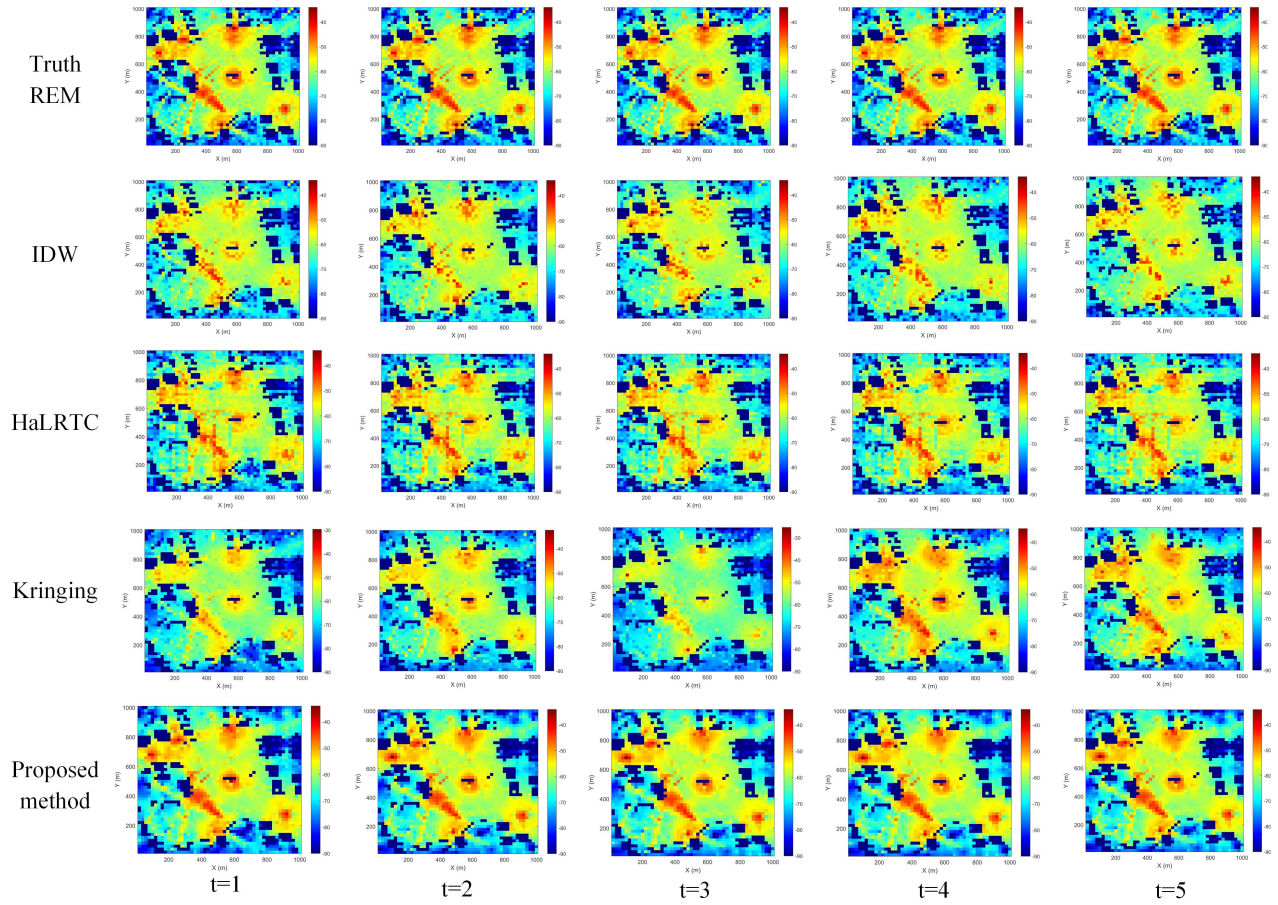


Fig. 9: Visualization of reconstructed REMs with different methods at five time instants.

reconstruction methods, the influence of sensor layout on the HaLRTC using the randomly layout scheme yields the best performance.

In order to obtain meaningful comparison results, we have obtained the performance of the proposed separate algorithms including sensor layout optimization (SLO), propagation dictionary improvement (PDI) and time-variant REM reconstruction (TVR). Fig. 8 presents the average MAE performance of different algorithms at different missing rate ranging from 10% (2250 sensors) to 90% (250 sensors). It is noted that both the proposed algorithms can improve the reconstruction performance compared to the basic TVR. The SLO-TVR outperforms TVR by 0.2-0.5 dBm, which shows that the sensor layout is vital for REM reconstruction, particularly when dealing with limited spectrum data. The PDI-TVR has better reconstruction performance due to the adopted propagation model considering various environmental factors. The best performance is achieved by the combination of the SLO and the PDI, and the corresponding method (SLO-PDI-TVR) outperforms the other algorithms by 0.2-1 dBm.

Fig. 9 presents the truth and reconstructed REMs at each time instant with 50% (1250 sensors) missing data where the dark blue regions represent areas obscured by buildings. The obtained results clearly show that the proposed methodology has the best performance compared with the other three methods. On the other hand, the IDW method lacks a robust

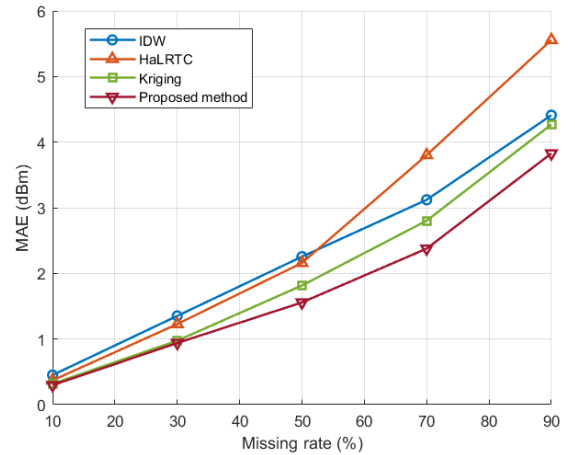


Fig. 10: Reconstruction performance comparisons of different methods with different missing rate.s

spatial-temporal distance metric and overly considers irrelevant data which results in poor reconstruction. Furthermore, the HaLRTC method addresses the completion problem by considering the correlation between rows and columns, which results in a distinct linear character to the reconstruction results. Finally, the Kriging method reconstructs REM based

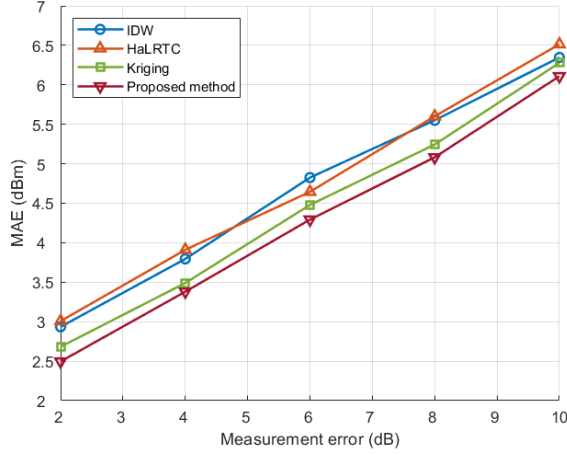


Fig. 11: Reconstruction performance comparisons of the four methods under consideration versus measurement error.

on spatial semi-variance function ignoring the data correlation of time dimension. Moreover, it fails to accurately model the realistic propagation process. To quantitatively analyze the reconstruction performance of these four methods, Fig. 10 presents their performance comparison by showing the average MAE performance at different missing rate ranging from 10% (2250 sensors) to 90% (250 sensors). These results clearly show that, as expected, the MAE of all methods increase as the missing rate increases. However, the proposed methodology outperforms the others by about 0.1-1.7 dBm. The Kriging method yields the second best performance, while HaLRTC outperforms IDW at the low missing rate. When the missing rate exceeds 50%, tensor completion shows a noticeable performance decline.

Measurement error caused by the sensor noise, which is assumed to be Gaussian with zero mean and variance between 2-10 dB, is another important factor affecting the reconstruction performance. Fig. 11 presents the reconstruction performance of the four methods with respect to different measurement error. Consistent with previous results, it increases almost linearly, with proposed method having the lowest reconstruction error, followed by the Kriging method, while the IDW and HaLRTC methods have similar performance.

B. Field Measurement Experiments

To experimentally validate the effectiveness of the proposed reconstruction methodology we have chosen a relatively open football field in the NUAU campus for field measurement experiments. As illustrated in Fig. 12, the field is made of artificial turf surrounded by a red rubber track, and four mobile RF emitters with the transmitting power of 10 dBm at 1300 MHz equipped with an isotropic antenna and a mobile power supply have been used. Taking the lower left corner as the origin of the football field, each RF emitter is marked in the figure where it is shown that RF 1 and RF 2 move to the right, RF 3 moves down, and RF 4 moves up. All the values of the important parameters used to carry out the field measurement experiments are shown in Table II.

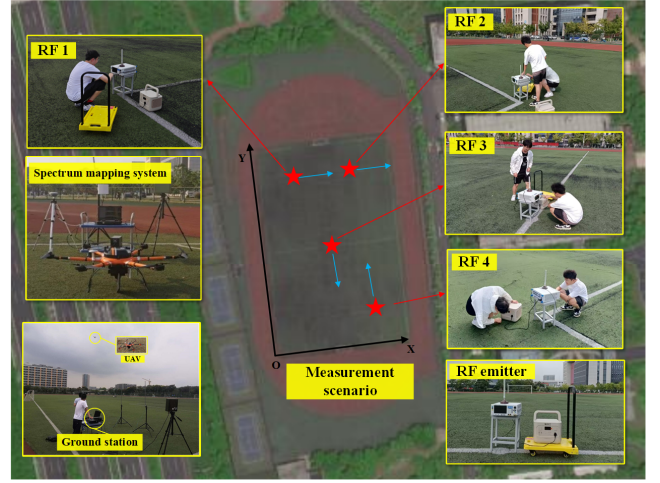


Fig. 12: A view of the football field where field measurement experiments took place.

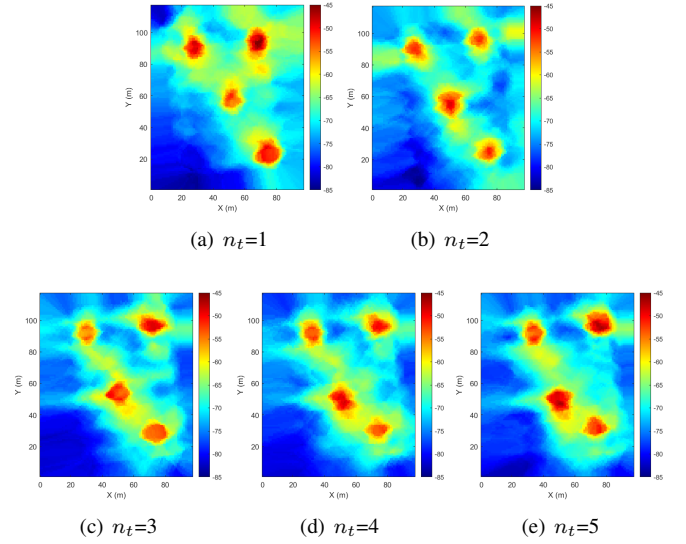


Fig. 13: Visualization of reconstructed REMs with field obtained experimental data.

The spectrum data is collected with a sampling rate of 25% via our own developed spectrum mapping system [38]. An unmanned aerial vehicle (UAV) equipped with a monitoring module was used to collect data, such as the RSS and GPS locations of the target area, and then transmitted these data to the ground station by the A2G communication module. The ground station processed and stored the received data, and subsequently the REM with missing data have been obtained.

Fig. 13 presents various experimentally reconstructed REMs at different time instants. These results clearly show that there are four red regions with high RSS values, which correspond to four RF emitters. The shape of each red region is an approximate circle due to the use of isotropic antennas. It can be also observed that the RSS weakens as the distance from the RF transmitter increases, which is consistent with the characteristic of signal attenuation during propagation. Furthermore, the obtained REMs clearly show the trend of

TABLE II: FIELD MEASUREMENT PARAMETERS

Parameter	Value					
	Index	Height (m)	Power (dBm)	Speed (m/s)	Antenna type	Antenna max gain (dBi)
RF emitter setting	1	1	10	1	Isotropic	0
	2	1	10	1	Isotropic	0
	3	1	10	1	Isotropic	0
	4	1	10	1	Isotropic	0
Center frequency	1.3 GHz					
Bandwidth	10 MHz					
Cartography area	110 m x 70 m					
Grid resolution	1 m x 1 m					
Update time interval	1 s					

RF transmitter movement, namely, the two RF transmitters above are moving to the right, while the two RF transmitters below are getting closer from the up-down sides, validating the effectiveness of the proposed methodology.

V. CONCLUSIONS

In this paper, we have proposed a time-variant REM reconstruction methodology under dynamically changing spectrum environments. The proposed scheme has modeled the reconstruction problem as a compressed sensing problem which mainly involves data sampling and recovery. Firstly, we have developed an optimization method to achieve a better spatial layout of distributed sensors. Secondly, through sampled data, the channel propagation model has been iteratively improved for building a realistic channel dictionary. Finally, by exploring the spatial-temporal correlation of spectrum data, a heterogeneous recovery method has been proposed to reconstruct the time-variant REM. The proposed method has been evaluated by simulation and shown to be superior to the baseline methods. The effectiveness has been also verified by field measurements in the campus scenario. In the future work, we will extend this scheme to the 4D REM reconstruction, i.e., 3D space domain and 1D time domain, and optimize the UAV trajectory based on the proposed sampling scheme.

APPENDIX A

PROOF OF THE EQUATION (30)

In practice, it can be addressed by applying the product sum model, which assumes independent spatiotemporal variation and reflect the heterogeneity of space and time domain. It is defined as

$$R_{st}(\Delta h_s, \Delta h_t) = k_1 R_s(\Delta h_s) R_t(\Delta h_t) + k_2 R_s(\Delta h_s) + k_3 R_t(\Delta h_t). \quad (35)$$

The spatial-temporal semi-variance can be derived as

$$\begin{aligned} \gamma_{st}(\Delta h_s, \Delta h_t) &= (k_1 R_t(0) + k_2) \gamma_s(\Delta h_s) + (k_1 R_s(0) + k_3) \gamma_t(\Delta h_t) \\ &\quad - k_1 \gamma_s(\Delta h_s) \gamma_t(\Delta h_t), \end{aligned} \quad (36)$$

where $R_s(\Delta h_s)$ and $R_t(\Delta h_t)$ are the space and time covariance, respectively, and $\gamma_s(\Delta h_s)$ and $\gamma_t(\Delta h_t)$ are the corresponding semi-variance functions.

The coefficients k_1 , k_2 and k_3 can be calculated by

$$\begin{cases} k_1 = [R_s(0) + R_t(0) - R_{st}(0)] / R_s(0) R_t(0) \\ k_2 = [R_{st}(0, 0) - R_t(0)] / R_s(0) \\ k_3 = [R_{st}(0, 0) - R_s(0)] / R_t(0) \end{cases}. \quad (37)$$

APPENDIX B

PROOF OF THE EQUATION (31)

Since minimizing the prediction variance of an unbiased predictor is equivalent to minimizing the mean squared error, we have

$$\begin{aligned} E(\hat{x} - x)^2 &= \sum_{i=1}^M \sum_{j=1}^M w_i w_j E(\tilde{x}_i \tilde{x}_j) - 2E(\sum_{i=1}^M w_i \tilde{x}_i x) + E(xx) \\ &= -\frac{1}{2} \sum_{i=1}^M \sum_{j=1}^M w_i w_j E[(\tilde{x}_i - \tilde{x}_j)^2] + \sum_{i=1}^M w_i E[(\tilde{x}_i - x)^2] \\ &= -\sum_{i=1}^M \sum_{j=1}^M w_i w_j \gamma_{st}(\Delta h_{sij}, \Delta h_{tij}) + 2 \sum_{i=1}^M w_i \gamma(\Delta h_{si0}, \Delta h_{ti0}), \end{aligned} \quad (38)$$

where $\gamma_{st}(\Delta h_{s1M}, \Delta h_{t1M})$ is the spatial-temporal semi-variance between \tilde{x}_1 and \tilde{x}_M . $\gamma_{st}(\Delta h_{s10}, \Delta h_{t10})$ is the spatial-temporal semi-variance between \tilde{x}_1 and arbitrary unknown position.

We obtain the constraints of coefficients as

$$\begin{aligned} E(\hat{x} - x) &= E(\sum_{i=1}^M w_i \tilde{x}_i - x) = E(\sum_{i=1}^M w_i b_i x_i - x) \\ &= E(x) \sum_{i=1}^M w_i b_i - E(x) = 0, \end{aligned} \quad (39)$$

Then we have

$$\sum_{i=1}^M w_i b_i = 1. \quad (40)$$

REFERENCES

- [1] R. Shrestha, D. Romero and S. P. Chepuri, "Spectrum surveying: Active radio map estimation with autonomous UAVs," *IEEE Transactions on Wireless Communications*, vol. 22, no. 1, pp. 627–641, 2023.
- [2] K. Mao, Q. Zhu, Y. Qiu, X. Liu, M. Song, W. Fan, A.B.J. Kokkeler, and Y. Miao, "A UAV-Aided Real-Time Channel Sounder for Highly Dynamic Non-Stationary A2G Scenarios," *IEEE Transaction on Instrument and Measurement*, vol. 72, pp. 1–15, 2023.
- [3] G. Ding, Q. Wu, L. Zhang, Y. Lin, T. A. Tsiftsis, and Y.-D. Yao, "An amateur drone surveillance system based on the cognitive internet of things," *IEEE Communications Magazine*, vol. 56, no. 1, pp. 29–35, 2018.
- [4] S. K. Sharma, E. Lagunas, S. Chatzinotas and B. Ottersten, "Application of compressive sensing in cognitive radio communications: A survey," *IEEE Communications Surveys & Tutorials*, vol. 18, no. 3, pp. 1838–1860, 2016.
- [5] H. B. Yilmaz, T. Tugcu, F. Alagöz, and S. Bayhan, "Radio environment map as enabler for practical cognitive radio networks," *IEEE Communications Magazine*, vol. 51, no. 12, pp. 162–169, 2013.
- [6] H. B. Yilmaz and T. Tugcu, "Location estimation-based radio environment map construction in fading channels," *Wireless communications & mobile computing*, vol. 15, no. 3, pp. 561–570, 2015.
- [7] C. He, Y. Dong, and Z. J. Wang, "Radio map assisted multi-UAV target searching," *IEEE Transactions on Wireless Communications*, vol. 22, no. 7, pp. 4698–4711, 2023.
- [8] H. Zhang, S. Peng, J. Zhang, and Y. Lin, "Big data analysis and prediction of electromagnetic spectrum resources: A graph approach," *Sustainability*, vol. 15, no. 1, p. 508, 2022.
- [9] Y. Huang, H. Cui, Y. Hou, C. Hao, W. Wang, Q. Zhu, J. Li, Q. Wu, and J. Wang, "Space-based electromagnetic spectrum sensing and situation awareness," *Space: Science & Technology*, vol. 4, p. 0109, 2024.
- [10] K. Manohar, B. W. Brunton, J. N. Kutz and S. L. Brunton, "Data-driven sparse sensor placement for reconstruction: Demonstrating the benefits of exploiting known patterns," *IEEE Control Systems Magazine*, vol. 38, no. 3, pp. 63–86, 2018.
- [11] H. Sun and J. Chen, "Propagation map reconstruction via interpolation assisted matrix completion," *IEEE Transactions on Signal Processing*, vol. 70, pp. 6154–6169, 2022.
- [12] D. Romero and S. -J. Kim, "Radio Map Estimation: A data-driven approach to spectrum cartography," *IEEE Signal Processing Magazine*, vol. 39, no. 6, pp. 53–72, 2022.
- [13] Z. El-friakh, A. M. Voicu, S. Shabani, L. Simić and P. Mähönen, "Crowd-sourced Indoor Wi-Fi REMs: Does the Spatial Interpolation Method Matter?," in *IEEE International Symposium on Dynamic Spectrum Access Networks (DySPAN)*, Seoul, Korea (South), 2018, pp. 1–10.
- [14] K. Sato, K. Suto, K. Inage, K. Adachi, and T. Fujii, "Space-frequency-interpolated radio map," *IEEE Transactions on Vehicular Technology*, vol. 70, no. 1, pp. 714–725, 2021.
- [15] M. Tang, G. Ding, Q. Wu, Z. Xue, and T. A. Tsiftsis, "A joint tensor completion and prediction scheme for multi-dimensional spectrum map construction," *IEEE Access*, vol. 4, pp. 8044–8052, 2016.
- [16] B. Khalfi, B. Hamdaoui, M. Guizani, and A. Elmaghub, "Scalable spectrum database construction mechanisms for efficient wideband spectrum access management," *Physical Communication*, vol. 46, p. 101318, 2021.
- [17] D. Schäufele, R. L. G. Cavalcante, and S. Mtanczak, "Tensor completion for radio map reconstruction using low rank and smoothness," in *IEEE 20th International Workshop on Signal Processing Advances in Wireless Communications (SPAWC)*, Cannes, France, 2019, pp. 1–5.
- [18] G. Zhang, X. Fu, J. Wang, and M. Hong, "Spectrum cartography via coupled block-term tensor decomposition," *IEEE Transactions on Signal Processing*, vol. 68, pp. 3660–3675, 2020.
- [19] X. Han, L. Xue, Y. Xu, and Z. Liu, "A two-phase transfer learning-based power spectrum maps reconstruction algorithm for underlay cognitive radio networks," *IEEE Access*, vol. 8, pp. 81232–81245, 2020.
- [20] R. Levie, Ç. Yapar, G. Kutyniok, and G. Caire, "RadioUNet: Fast radio map estimation with convolutional neural networks," *IEEE Transaction on Wireless Communication*, vol. 20, no. 6, pp. 4001–4015, 2021.
- [21] S. Roger, M. Brambilla, B. C. Tedeschini, C. Botella-Mascarell, M. Cobos, and M. Nicoli, "Deep-learning-based radio map reconstruction for V2X communications," *IEEE Transactions on Vehicular Technology*, vol. 73, no. 3, pp. 3863–3871, 2023.
- [22] S. Shrestha, X. Fu and M. Hong, "Deep Spectrum Cartography: Completing radio map tensors using learned neural models," *IEEE Transactions on Signal Processing*, vol. 70, pp. 1170–1184, 2022.
- [23] G. Chen, Y. Liu, T. Zhang, J. Zhang, X. Guo and J. Yang, "A Graph Neural Network Based Radio Map Construction Method for Urban Environment," *IEEE Communications Letters*, vol. 27, no. 5, pp. 1327–1331, 2023.
- [24] H. Zou, C. Chen, M. Li, J. Yang, Y. Zhou, L. Xie, and C. J. Spanos, "Adversarial learning-enabled automatic WiFi indoor radio map construction and adaptation with mobile robot," *IEEE Internet of Things Journal*, vol. 7, no. 8, pp. 6946–6954, 2020.
- [25] M. Pesko, T. Javornik, L. Vidmar, A. Kosir, M. Stular, and M. Mohorcic, "The indirect self-tuning method for constructing radio environment map using omnidirectional or directional transmitter antenna," *EURASIP Journal on Wireless Communications and Networking*, vol. 2015, no. 1, pp. 1–12, 2015.
- [26] E. Yang, H. Yu, X. Mo and A. Gao, "Construction of wideband radio environment map based on compressed sensing," in *International Conference on Wireless Communications and Signal Processing (WCSP)*, Nanjing, China, 2022, pp. 444–449.
- [27] M. A. Jeison, M. T. Jose, A. F. Henry, and A. Leonardo, "Compressive multispectral spectrum sensing for spectrum cartography," *Sensors*, vol. 18, no. 2, p. 387, 2018.
- [28] F. Shen, Z. Wang, G. Ding, K. Li and Q. Wu, "3D compressed spectrum mapping with sampling locations optimization in spectrum-heterogeneous environment," *IEEE Transactions on Wireless Communications*, vol. 21, no. 1, pp. 326–338, 2022.
- [29] J. Wang, Q. Zhu, Z. Lin, Q. Wu, Y. Huang, X. Cai, W. Zhong, and Y. Zhao, "Sparse bayesian learning-based 3D spectrum environment map construction-sampling optimization, scenario-dependent dictionary construction and sparse recovery," *IEEE Transactions on Cognitive Communications and Networking*, vol. 10, no. 1, pp. 80–93, 2024.
- [30] J. Wang, Q. Zhu, Z. Lin, J. Chen, G. Ding, Q. Wu, G. Gu, and Q. Gao, "Sparse bayesian learning-based hierarchical construction for 3D radio environment maps incorporating channel shadowing," *IEEE Transactions on Wireless Communications*, early access, 2024, doi: 10.1109/TWC.2024.3416447.
- [31] Y. Hu and R. Zhang, "A spatial-temporal approach for secure crowd-sourced radio environment map construction," *IEEE/ACM Transactions on Networking*, vol. 28, no. 4, pp. 1790–1803, 2020.
- [32] M. S. Rahman, H. Gupta, A. Chakraborty, and S. Das, "Creating spatial-temporal spectrum maps from sparse crowdsensed data," in *IEEE Wireless Communications and Networking Conference (WCNC)*, Marrakesh, Morocco, 2019, pp. 1–7.
- [33] X. Li, X. Wang, T. Song and J. Hu, "Robust online prediction of spectrum map with incomplete and corrupted observations," *IEEE Transactions on Mobile Computing*, vol. 21, no. 12, pp. 4583–4594, 2022.
- [34] F. Shen, G. Ding, and Q. Wu, "Time-variant spectrum mapping via reduced basis representation and greedy sampling locations optimization," *IEEE Communications Letters*, vol. 27, no. 3, pp. 991–995, 2023.
- [35] P. Zhen, B. Zhang, C. Xie, and D. Guo, "A radio environment map updating mechanism based on an attention mechanism and siamese neural networks," *Sensors*, vol. 22, no. 18, p. 6797, 2022.
- [36] Y. Zhao, Q. Zhu, Z. Lin, L. Guo, Q. Wu, J. Wang, and W. Zhong, "Temporal prediction for spectrum environment maps with moving radiation sources," *IET Communications*, vol. 17, no. 5, pp. 538–548, 2022.
- [37] H. Ni, Q. Zhu, B. Hua, K. Mao, Y. Pan, F. Ali, W. Zhong, and X. Chen, "Path loss and shadowing for UAV-to-Ground UWB channels incorporating the effects of built-up areas and airframe," *IEEE Transactions on Intelligent Transportation Systems*, 2024, doi: 10.1109/TITS.2024.3418952.
- [38] Q. Zhu, Y. Zhao, Y. Huang, Z. Lin, L. H. Wang, Y. Bai, T. Lan, F. Zhou, and Q. Wu, "DEMO Abstract: An UAV-based 3D spectrum real-time mapping system," in *IEEE Conference on Computer Communications Workshops (INFOCOM WKSHPS)*, New York, NY, USA, 2020. pp. 1–2.



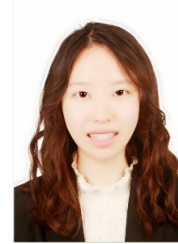
Qinhao Gao received the B.S. degree in communication engineering from the School of Internet of Things Engineering, Jiangnan University, Wuxi, China, in 2023. He is currently pursuing the Ph.D. degree in communications and information systems with College of Electronic and Information Engineering, Nanjing University of Aeronautics and Astronautics. His current research direction is related to spectrum mapping.



Qiuming Zhu received his BS in electronic engineering from Nanjing University of Aeronautics and Astronautics (NUAA), Nanjing, China, in 2002 and his MS and PhD in communication and information system from NUAA in 2005 and 2012, respectively. Since 2021, he has been a professor in the Department of Electronic Information Engineering, NUAA. From Oct. 2016 to Oct. 2017, June 2018 to Aug. 2018 and June 2018 to Aug. 2018, he was also an academic visitor at Heriot-Watt University, Edinburgh, U. K. He has authored or coauthored more than 160 articles in refereed journals and conference proceedings. He holds over 50 China and international patents. His current research interests include channel sounding, modeling, and emulation for the fifth/sixth generation (5G/6G) mobile communication and unmanned aerial vehicles (UAV) communication systems, 3D spectrum mapping and environment awareness.



Yang Huang received the B.S. and M. S. degrees from Northeastern University, China, in 2011 and 2013, respectively, and the Ph.D. degree from Imperial College London in 2017. He is currently an Associate Professor with College of Electronic and Information Engineering, Nanjing University of Aeronautics and Astronautics, Nanjing, China. His research interests include wireless communications, MIMO systems, convex optimization, machine learning and signal processing for communications. He has served as Technical Program Committee (TPC) members for many International conferences, such as IEEE GLOBECOM, *etc.*



Jie Wang received the B.S. degree in internet of things engineering from the College of Information Science and Technology, Nanjing Forestry University of China, Nanjing, China, in 2021. She is currently pursuing the Ph.D. degree in communications and information systems with the College of Electronic and Information Engineering, Nanjing University of Aeronautics and Astronautics. Her current research interests conclude spectrum mapping.



UAV communications.

Zhipeng Lin received the Ph.D. degrees from the School of Information and Communication Engineering, Beijing University of Posts and Telecommunications, Beijing, China, and the School of Electrical and Data Engineering, University of Technology of Sydney, NSW, Australia, in 2021. Currently, He is an Associate Researcher in the College of Electronic and Information Engineering, Nanjing University of Aeronautics and Astronautics, Nanjing, China. His current research interests include signal processing, massive MIMO, spectrum sensing, and



Qihui Wu received the B.S. degree in communications engineering and the M.S. and Ph.D. degrees in communications and information system from the PLA University of Science and Technology, Nanjing, China, in 1994, 1997, and 2000, respectively. He is currently a Professor with the College of Electronic and Information Engineering, Nanjing University of Aeronautics and Astronautics. His current research interests include algorithms and optimization for cognitive wireless networks, soft-defined radio, and wireless communication systems.



P. Takis Mathiopoulos is a professor of telecommunications at the Department of Informatics and Telecommunications, National and Kapodistrian University of Athens, 15784 Athens, Greece. He received his Ph.D. degree from the University of Ottawa, Canada. His current research interests include wireless terrestrial and satellite communication systems/networks as well as remote sensing, lidar systems, and information technology, including blockchain systems. He is a Life Senior Member of IEEE.



Yi Zhao received the B.S. degree in information engineering from Nanjing University of Aeronautics and Astronautics (NUAA) in 2021. He is currently working towards the master degree in electronic information engineering, NUAA. His current research is temporal and spatial prediction and reconstruction of spectrum situation.